Analytica Chimica Acta 1092 (2019) 85–92

Contents lists available at ScienceDirect

Analytica Chimica Acta

journal homepage: www.elsevier.com/locate/aca

Using PbS–Au heterodimers as signal quencher for the sensitive photoelectrochemical immunoassay of amyloid β-protein

Qingzhi Han, Huitong Chi, Hanyu Wang, Dan Wu*, Qin Wei

Key Laboratory of Interfacial Reaction & Sensing Analysis in Universities of Shandong, School of Chemistry and Chemical Engineering, University of Jinan, Jinan, 250022, PR China

HIGHLIGHTS

- PbS–Au heterodimers were used as novel signal quencher to quench the PEC signal of TiO_2/BiOI heterostructure (p-n).
- The Au in PbS–Au heterodimers could expedite the electron separation/transfer process and connected with Ab_2.
- The biosensor showed a low LOD of 0.028 pg/mL and a wide detection range of 0.0001–500 ng/mL.

GRAPHICAL ABSTRACT

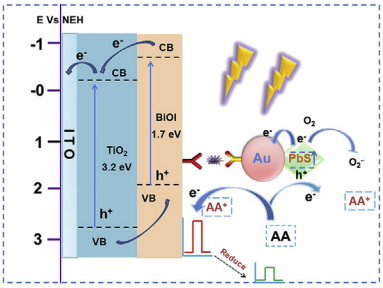

ARTICLE INFO

Article history:
Received 21 August 2019
Received in revised form
13 September 2019
Accepted 14 September 2019
Available online 16 September 2019

Keywords:
PbS–Au heterodimers
Photoelectrochemical
Amyloid β-protein
TiO_2/BiOI heterostructure
Signal quencher

ABSTRACT

By using PbS–Au heterodimers as the signal quencher, TiO_2/BiOI as matrix, a novel sandwich-type photoeletrochemical (PEC) biosensor for sensitive determination of amyloid β-protein (Aβ, ~4 KDa) was developed. BiOI was attached to the surface of TiO_2 and formed a heterogeneous structure (p-n junction), which enlarged the light harvest range and enhanced the electron transfer rate of TiO_2. In order to quench the PEC signal, PbS–Au heterodimers were used as the labels to combine with Aβ. Owing to the competitively light energy harvesting and electron donor consuming effect of PbS–Au heterodimers, less light energy and electron donor arrived at TiO_2/BiOI. In addition, Au directly contacted with PbS could enhance the electron seperation and transfer rate, and lead to improved competitiveness consumption of the electron donor. PbS–Au integrated with secondary antibodies formed PbS–Au-Ab_2 bioconjugate, which would further obstruct the electron transfer and impede the interreaction between electron donor and photoelectrode surfaces. Owing to the unique PbS–Au heterodimer structure and the quenching effect of PbS–Au-Ab_2 bioconjugate, the fabricated immunosensor for Aβ detection exhibited good stability, high sensitivity, and a low detection limit of 0.028 pg/mL (S/N = 3).

1. Introduction

Alzheimer's disease (AD) is a common chronic neurodegenerative disease, and one of the most common diseases in the entire world. The clinicopathological characteristics of AD include neuritic plaques composed of aggregated amyloid-β peptides surrounded by dystrophic neurites, also accompanied by neuronal and synaptic degeneration [1,2]. Based on research findings, amyloid β-protein (Aβ, ~4 KDa) is derived from hydrolyzed β-amyloid precursor protein (secreted by cell), and has a strong neurotoxic effect after the accumulation in matrix [3–5]. Therefore, Aβ can be used as one

* Corresponding author.
E-mail address: wudan791108@163.com (D. Wu).

https://doi.org/10.1016/j.aca.2019.09.041
0003-2670/

kind of specific biomarkers for AD detection [6], and various methods have been developed for the Aβ detection [2,6,7]. The photoelectrochemical (PEC) immunosensor is derived from electrochemical immunosensor, in which the light and electricity are used as separated excitation and detection signals, respectively [8,9]. The PEC bioanalysis also inherits the advantages of traditional electrochemical bioanalysis, such as cost efficiency and simple instrumentation [10–13]. In consideration of these merits, we developed a PEC sensing platform for the Aβ detection by monitoring the biological/chemical interactions generated signal changes.

As we all known, sensitivity is a very important evaluation index for the performance of PEC biosensor [14,15]. Various methods have been used to improve the sensitivity of the PEC biosensor [16–18]. Among them, using p-type semiconductor as signal quencher to compete with n-type semiconductor for the consuming of electron donor is a powerful and promising way [19–21]. PbS is a typical p-type semiconductor, on account of its large exciton Bohr radius, high dielectric constant, carrier mobility as well as strong electron carriers confinement effects [22–24], which can generate multiple electron-hole pairs. What's more, compared with n-type semiconductors, p-type PbS is more apt to interact with O_2 (electron acceptor) rather than electron donor (e.g. AA) in the electrolyte (PBS) [19,25]. In addition, PbS has a narrower band-gap (~0.44 eV) [26], which makes it has a wide light absorption capacity. Therefore, PbS is an appropriate p-type semiconductor for the quenching of PEC signals. Under continuous light irradiation, the photoinduced electron of PbS could be captured by O_2 (dissolved in electrolyte), and the photogenerated hole (in the valence band) could reacted with the electron donor (ascorbic acid) in the meantime. For the above reasons, in the PEC sensing system, PbS could be used to compete with the matrix materials to consume the electron donor. In addition, combining PbS with Au together could form PbS–Au heterodimer [27], and the quenching efficiency of PbS also could be improved. The reason is that Au nanoparticle (metallic nanostructure) directly contacted with PbS (semiconductor) forms a metal/semiconductor junction enhanced its electron/hole separation and transportation (photoactivity) rate [28]. Moreover, thanks to the good biocompatibility of Au, PbS–Au could directly bind with secondary antibodies (Ab_2) and need not further modification [29].

Titania (TiO_2) as a popular wide band-gap (~3.2 eV) semiconductor, owing to its cost efficient, good chemical stability and nontoxic properties, has attracted increasing attention [30–34]. Bismuth oxyiodide (BiOI), as an important inorganic semiconductor with a narrow band-gap of ~1.7 eV, has already been wildly used in the promising industrial applications owing to its excellent photocatalysis and unique optical properties [35–38]. By combining the wide band-gap semiconductor TiO_2 and narrow band-gap BiOI together, Zhang et al. [39] developed a TiO_2/BiOI heterostructure, which showed better photocatalytic activities compared with pure TiO_2 or BiOI, indicating that under the illumination of visible light BiOI and TiO_2 have well matched banding energy (more efficient generation and separation of electron/hole pairs). Furthermore, as an easy synthesized material (by using solvothermal or hydrothermal method), BiOI also is a popular sensitizers, which could form heterostructures with TiO_2. Nevertheless, the previous research is mainly about its photocatalytic or photovoltaic applications.

In the present work, we developed a novel sandwich-type immunosensor for Aβ detection, which was fabricated by using TiO_2/BiOI heterostructure as matrix and PbS–Au as quencher. BiOI nanosheet was decorated on the surface of TiO_2 nanosphere by the chemical bath deposition (CBD) method and the thickness of BiOI could be adjusted by different repeating cycles of CBD process. PbS–Au heterodimers as labels could compete with the matrix and further quench the output PEC signals. What's more, the unique PbS–Au heterodimers, to the best of our knowledge, hasn't been used in the field of PEC immunoassay.

2. Experimental section

Reagents, apparatus as well as the preparation of ITO/TiO_2, ITO/TiO_2/BiOI/CS-GA electrode, PbS octahedron, PbS–Au octahedron-nanoparticle heterodimers and PbS–Au-Ab_2 bioconjugate are included in the Supporting Information.

2.1. Fabrication of the PEC biosensor

The fabrication procedure of the PEC biosensor was shown in Scheme 1. First, 5 μL of Ab_1 (10 μg/mL) was dropped onto the surface of the as prepared ITO/TiO_2/BiOI/PDA/CS-GA electrode and incubated at 4 °C for 120 min, and following rinsed with PBS (0.1 mol/L, pH = 7.4) to wash off physically absorbed Ab_1. Then the resulting electrode was incubated with 5 μL of BSA (1 wt%) for 120 min to block possible remaining active sites. Next, 5 μL of different concentrations of Aβ was added and incubated at 4 °C for 120 min. After that, 5 μL of PbS–Au-Ab_2 (1 mg/mL) was added onto the as-prepared electrode to form the PEC biosensor. Following, it was washed with PBS solution thoroughly (removing non-specific absorption) to obtain the desired PEC biosensor.

2.2. PEC measurement procedure

Detection of Aβ was carried out through an electrochemical workstation in 0.1 mol/L PBS (pH = 7.4; containing 0.1 mol/L AA as the sacrificial electron donor) solution. The photocurrent was presented by the time-based photocurrent curve on a PEC workstation with 0 V applied potential and a LED light excitation source of 430 nm (light intensity is 180 W m^{-2}). The error bars in this work originated from three times of parallel measurement.

3. Results and discussion

3.1. Characterization of TiO_2, TiO_2/BiOI, PbS–Au heterodimers and PbS–Au-Ab_2 bioconjugate

Fig. 1A showed a typical SEM image of the TiO_2 nanoparticles, which have a diameter about 20 nm (inset is the picture of ITO/TiO_2). Fig. 1B exhibited the SEM image of BiOI modified TiO_2 (inset is the optical photograph of ITO/TiO_2/BiOI and SEM of magnified TiO_2/BiOI), as we can see, the BiOI nanosheets (~500 nm) were vertically decorated on the surface of TiO_2. The corresponding XRD patterns for TiO_2 (Fig. 1A) and TiO_2/BiOI (Fig. 1B) were shown in Fig. S1 (Supporting Information). The related XRD patterns shows that the main peaks of TiO_2 corresponding to anatase TiO_2 (JCPDS PDF#21–1272), while the pattern of TiO_2/BiOI contains both the main peaks of TiO_2 as well as BiOI (JCPDS PDF#10–0445), which proofs the successful synthesis of TiO_2/BiOI heterostructure. As seen from the EDS image of TiO_2/BiOI heterostructure nanocrystals in Fig. 1C, the element of Bi, O, I, and Ti are corresponding to the TiO_2/BiOI heterostructure, which indicating the successful synthesis of the sample. As shown in the TEM image (Fig. 1D), the PbS exhibited a octahedral structure with the size of ~50 nm. The UV–vis–NIR absorption spectrum and the Kubelka-Munk plots of PbS were shown in Fig. S2, from which we could see that PbS has a wide light absorption range and a narrow band-gap about 0.44 eV. The obtained PbS–Au heterodimers (Fig. 1E) presented a dumbbell-style structure, with a size about 140 nm (as shown in the inset of 1E: Au ~ 90 nm, PbS ~50 nm). Fig. 1F shows the XRD patterns of PbS

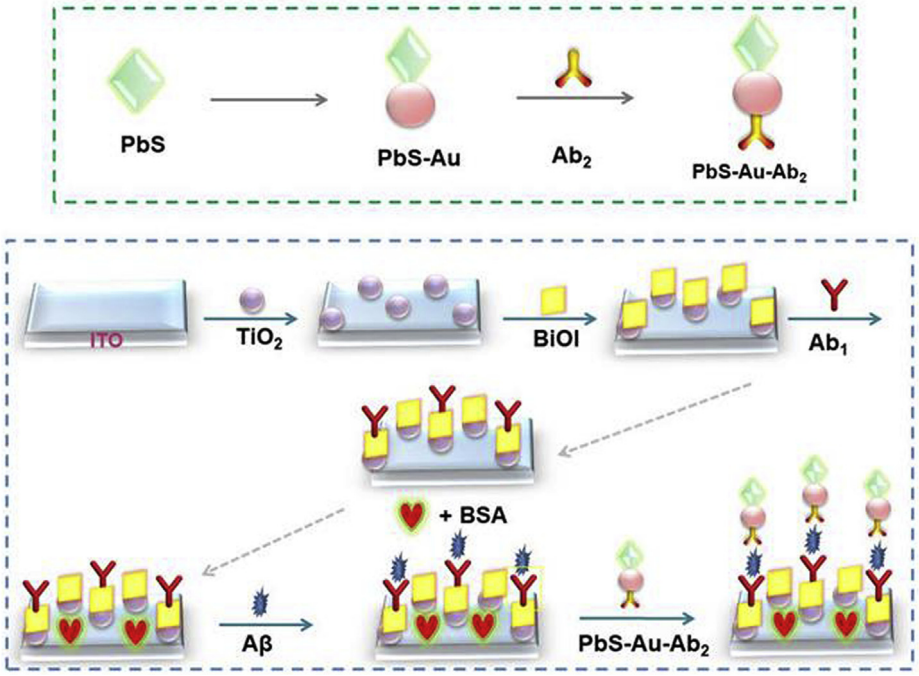

Scheme 1. Fabrication process of the proposed PEC biosensor.

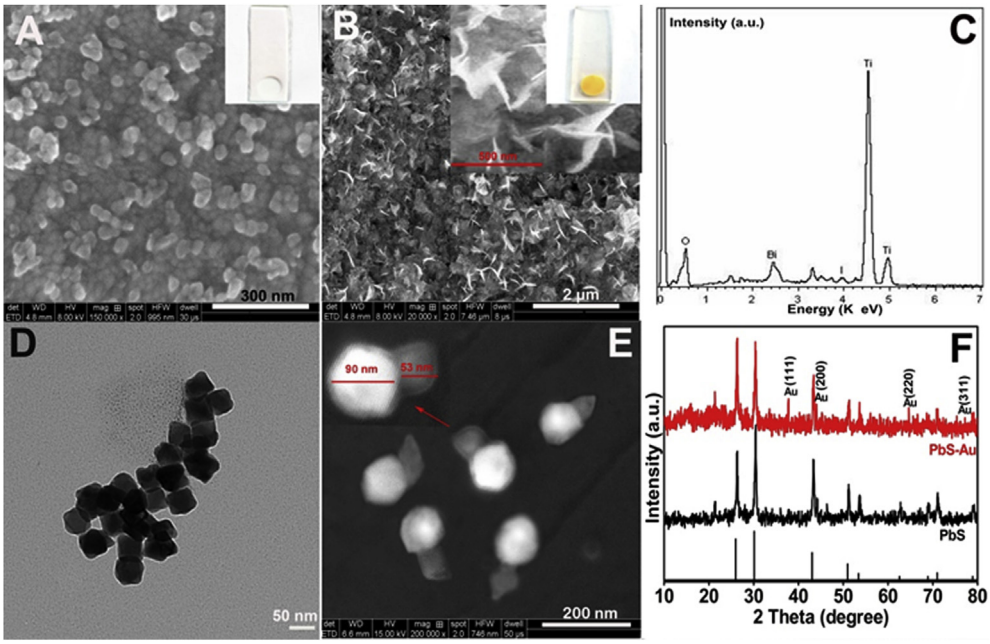

Fig. 1. SEM images of (A) TiO_2 nanoparticles (inset is the picture of ITO/TiO_2) and (B) TiO_2/BiOI heterostructure (inset is the optical photograph of ITO/TiO_2/BiOI and SEM of magnified TiO_2/BiOI). (C) EDS image of TiO_2/BiOI heterostructure. (D) TEM image of PbS octahedron. (E) SEM image of PbS–Au heterodimers. (F) XRD patterns of PbS (black curve) and PbS–Au (red curve) heterodimers. (For interpretation of the references to colour in this figure legend, the reader is referred to the Web version of this article.)

and PbS–Au. The related XRD pattern shows the main peaks corresponding to galena PbS with a octahedral structure (JCPDS PDF#05–0592) and gold (JCPDS PDF#04–0784), which demonstrated the successful synthesis of PbS–Au heterodimers.

The morphologies and microstructures of PbS–Au heterodimers were also confirmed by the TEM image. As shown in Fig. S3 A, the morphology of PbS–Au in agreement with the SEM image in Fig. 1E, indicating the successful synthesis of PbS–Au heterodimers. In addition, the UV–visible absorption spectroscopy of PbS–Au and PbS–Au-Ab_2 bioconjugate were used to demonstrate the interaction between PbS–Au heterodimers and Ab_2. Fig. S3 B illustrated the UV–visible absorption spectra of PbS–Au (black curve) heterodimers and PbS–Au-Ab_2 bioconjugate (red curve), respectively. The PbS–Au heterodimers and PbS–Au-Ab_2 bioconjugate both exhibited a peak at approximately 525 nm, which could be ascribed to the surface plasmon

resonance peak of the Au nanoparticles. Compared with PbS–Au heterodimers, a peak was observed at ~272 nm after PbS–Au had been conjugated with Ab_2, which could be ascribed to Ab_2. In addition, slight shift of the absorption band toward a higher wavelength (535 nm) was noticed, which suggested that PbS–Au and Ab_2 could form PbS–Au-Ab_2 bioconjugate.

XPS was performed to study the surface chemical compositions and oxidation states of the TiO_2/BiOI heterostructure. Fig. 2A shows the survey XPS spectrum of the as-fabricated TiO_2/BiOI heterostructure with the relevant elements of Bi, O, I, Ti, and C. The corresponding XPS spectra of Bi 4f, O 1s, I 3d, and Ti 2p are also illustrated. Fig. 2B shows the Bi $4f_{7/2}$ and Bi $4f_{5/2}$ signal with maxima located at ~158 and ~161 eV, while Fig. 2C indicates the O 1s peaks located at around ~529 and ~532 eV, which should be assigned to the TiO_2 and BiOI compound. Fig. 2D exhibits that I 3d have several peaks in the binding energies (BEs) of 615–635 eV. Specifically, the peaks centered at ~631 and ~619 eV could be attributed to I $3d_{3/2}$ and I $3d_{5/2}$, respectively. Fig. 2E of the Ti 2p spectrum exhibits a peaks at the BEs of ~459 eV. The peak positions were determined with a C 1s BEs of 284.6 eV (Fig. 2 F) as the internal benchmark. These results confirmed the successful preparation of TiO_2/BiOI heterostructure.

3.2. Mechanism of the as prepared PEC biosensor

Scheme 2 illustrated the mechanisms of the photocurrent generating and quenching of the fabricated PEC biosensor. TiO_2 is a popular wide band-gap semiconductor, modified with BiOI could promote its electron separation and light utilization efficiency. After the signal-quenching PbS–Au (p-type PbS, band-gap ~0.44 eV) heterodimers were introduced, the photocurrent would decrease. This could be explained as follows: First, the steric hindrance of

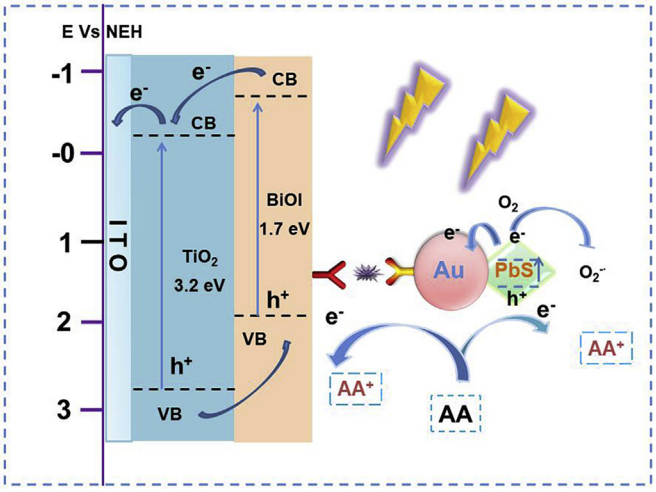

Scheme 2. Schematic illustration of the possible electron transfer mechanism of the "signal-off" PEC biosensor.

PbS-Ab_2 could hinder the electron transfer and reduce the photocurrent response. Second, the photoinduced electron of PbS were captured by the dissolved oxygen (electron acceptors) in electrolyte to form O_2^{-}·, and then the photoinduced hole was neutralized by ascorbic acid (AA), which would partly reduce the AA supplied for TiO_2/BiOI heterostructure as well as the photocurrent response [19,22]. Third, the direct contact between PbS and Au could expedite the electron separation and transfer process, which would further enhance the quenching effect. Hereto, a novel and effective quenching type PEC immunosensor was obtained.

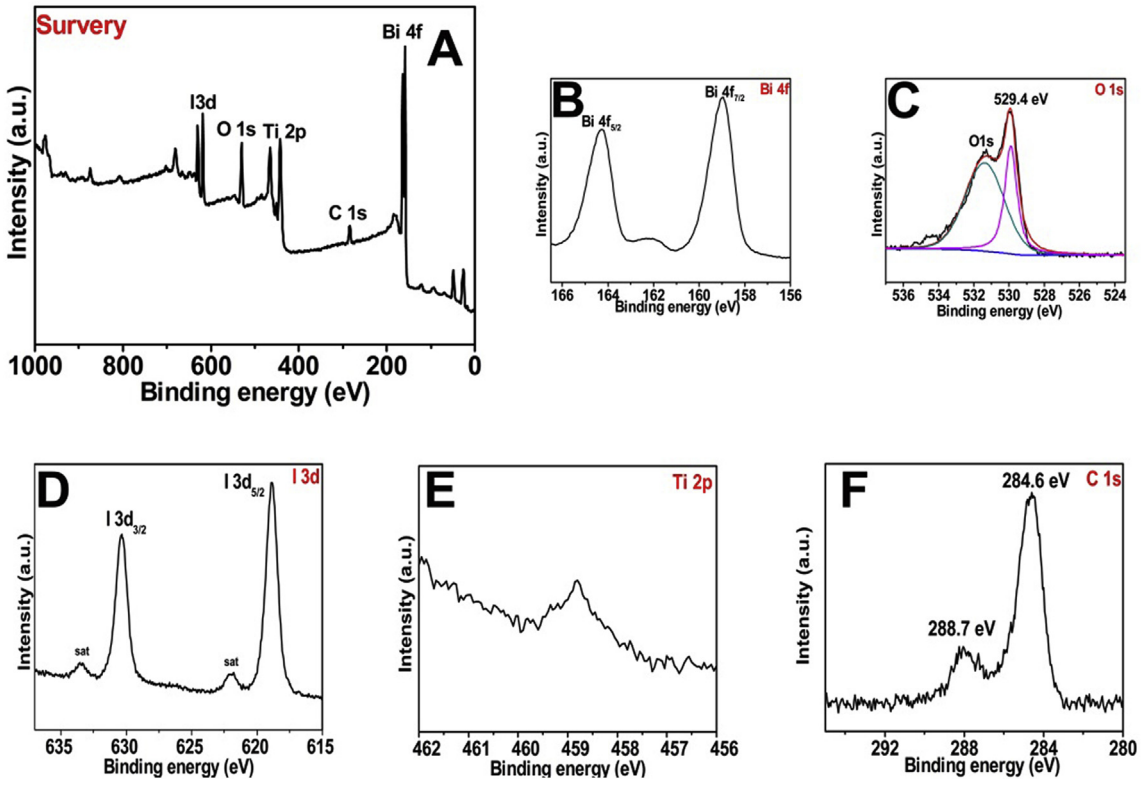

Fig. 2. (A) XPS spectrum of the as-fabricated TiO_2/BiOI heterostructure and (B–F) XPS spectra of Bi 4f, O 1s, I 3d, Ti 2p and C 1s, respectively.

3.3. Optimization of the experimental conditions

For the purpose of acquire an optimal output PEC signals, some detailed experimental conditions for the design of this sandwich-type biosensor were studied. Herein, we investigated the effect of TiO_2 concentration, CBD repeating cycles as well as the concentration of PbS–Au heterodimers on the photocurrent response of the sandwich-type immunosensing system. As indicated from Fig. S4 A, the photocurrent increased with the increasing TiO_2, and reached a relatively larger and stable photocurrent at 7 mg/mL. When the concentrations of TiO_2 exceed 7 mg/mL, TiO_2 falls off from the ITO more easily and its photocurrent also becomes unstable. Thus, 7 mg/mL was selected for the preparation of PEC biosensor. As seen from Fig. S4 B, with the increases of CBD repeating cycles, the photocurrent reached a maximum sensitization effect at 4 cycles. But when the repeating cycles exceed 4, the photocurrent decreased gradually, which could be attributed to the increased resistance with the excessive addition of BiOI. To simplify the process, 4 CBD repeating cycles was used for the preparation of TiO_2/BiOI heterostructure.

Figure S4 C gives the relationship between the PbS–Au-Ab_2 concentration and photocurrent. As shown in Fig. S4 C, the photocurrent gradually decreased with the increasing concentrations of PbS–Au-Ab_2 from 0.2 mg/mL to 1.0 mg/mL, and reached a plateau at 1 mg/mL. In consideration of the cost and material saving, 1 mg/mL of PbS–Au-Ab_2 was used for the preparation of PEC biosensor.

For comparison, pure BiOI coated on ITO was also prepared by the CBD method and with the same cycles. The different photocurrents response and UV–vis diffuse reflectance spectra of different electrodes were depicted in Figs. S5 and S6, respectively. Clearly, the photocurrent of TiO_2/BiOI (curve c) was much higher than pure BiOI (curve a) and TiO_2 (curve b) (shown in Fig. S5). This could be attributed to the well-matched band-structures of TiO_2 and BiOI, which effectively promoted the transfer rate of photogenerated electron and limited the electron/hole recombination rate. Fig. S6 shows the UV–vis diffuse reflectance spectra of pure TiO_2, pure BiOI and TiO_2/BiOI heterostructure. The spectrum depicted that the TiO_2 nanoparticles primarily absorb the ultraviolet light with a wavelength under 400 nm, which was ascribed to the wide band-gap absorption of TiO_2. After the modification of BiOI, the absorption edge was expanded to about 550 nm, which can be assigned to the inherent band-gap absorption of BiOI. This property enhances the utilization rate of TiO_2/BiOI to visible light, and as a result, the photocurrent also was enhanced [40].

3.4. Electrochemical characterizations of the proposed PEC biosensor

As shown in Fig. 3, the PEC responses of the electrode at different modification steps were investigated. Each step in the PEC sensor construction process could be reflected by the corresponding photocurrent responses. As depicted in Fig. 3A, the photocurrent increased from curve a (ITO electrode) to curve c (ITO/TiO_2/BiOI electrode). The increase could be attributed to that the TiO_2/BiOI heterostructure enhanced the electron transfer rate and depressed the electron-hole recombination efficiency. After the ITO/TiO_2/BiOI electrode was modified with CS-GA (cross-linking agent), Ab_1, BSA (blocking nonspecific site), Aβ, and PbS–Au-Ab_2 in sequence, the photocurrent decreased gradually. The reason is that the immobilized insulation substance (CS-GA and other proteins) increased the electron transfer resistance and impeded the electron donor to the electrode surface, as well as the quenching effect of PbS.

The fabrication process of the PEC biosensor was also investigated by the electrochemical impedance spectroscopy (EIS). The employed frequency range of EIS spectra was $0.1–1 \times 10^5$ Hz. Fig. 3B illustrated the Nyquist plot of different modified stages. As depicted in the graph, the impedance spectrum composed of a semicircle portion and a linear portion. The semicircle portion equals to the electron transfer resistance (R_{et}), and reflects the restricted diffusion of the redox probe through the multilayer system. The lower right inset in Fig. 3B is the equivalent circuit, containing the solution resistance (R_s), R_{et}, Warburg impedance (Z_w) and double layer capacitance (C_{dl}). The R_{et} indicates the electrode interfaces properties among other impedance composition. All of the above mentioned values were simulated by ZSimpWin (software) and exhibited in Table S1. As shown in Fig. 3B, the semicircle part increased from curve (a) to curve (h), which indicates the success modification of each step. The results agreed with the photocurrent change in Fig. 3A, which indicating the PEC biosensor was successfully constructed.

3.5. Analytical performance of the proposed PEC biosensor

To investigate the analytical performance of the PEC biosensor, the quantitative measurement was implemented by detecting Aβ with different concentrations under the optimized experiment conditions. The photocurrent response of the immunosensor could reflect the concentration of Aβ. Fig. 4A demonstrated that the photocurrent decreased with the increase of Aβ. As depicted in Fig. 4B, the photocurrent response linearly decreased with the increasing logarithm of Aβ concentration in the range of 1×10^{-4} ng/mL - 500 ng/mL. The calibration equation was $\Delta I = -0.6 \lg c$ - 2.4, with the correlation coefficient of 0.993. With the concentration of Aβ increased, a growing number of PbS–Au-Ab_2 bioconjugate was specifically bounded with Aβ (on the electrode surface), which consumed more electron donor (AA) and increased the electron transfer resistance, resulting in the reduced photocurrent. As shown in Table S2, our work showed a wide linear range and a low limit of detection, exhibiting its advantages in Aβ analysis.

To investigate the selectivity of the proposed PEC biosensor, the anti-interference test was carried out. There were several representative interfering proteins, involving prostatic specific antigen (PSA), carcino embryonie antigen (CEA) and immunoglobulin G (IgG) were used for the test. All the samples were measured under identical experimental condition. The specificity of the biosensor was appraised by measuring the photocurrent response of (a) blank, (b) 10 ng/mL PSA, (c) 10 ng/mL CEA, (d) 10 ng/mL IgG, (e) 10 ng/mL Aβ, and the mixture (f) (containing 10 ng/mL of Aβ, 10 ng/mL of PSA, 10 ng/mL of CEA and 10 ng/mL of IgG), respectively. Compared with the blank specimen, no obvious photocurrent changes appeared after the addition of PSA, CEA and IgG, as depicted in Fig. 4C. What's more, the photocurrent response toward the mixture (f) was approached to that incubating with 10 ng/mL Aβ. Therefore, the selectivity of the proposed PEC biosensor toward Aβ detection had acceptable performance. The stability of the PEC immunosensor was also an important criterion factor of the biosensor [41]. Fig. 4D exhibited the photocurrent response of the PEC immunosensor under “off-on-off” irradiation cycles for 480 s. As depicted in the chart, there was no distinct photocurrent change between each single “off-on-off” cycle, which demonstrated that the proposed PEC biosensor have a stable signal output capability.

3.6. Application of the proposed biosensor in ACSF samples

To prove the potential of the constructed biosensor in Alzheimer's disease detection, the recovery experiment was carried out by adding different concentrations of Aβ into artificial

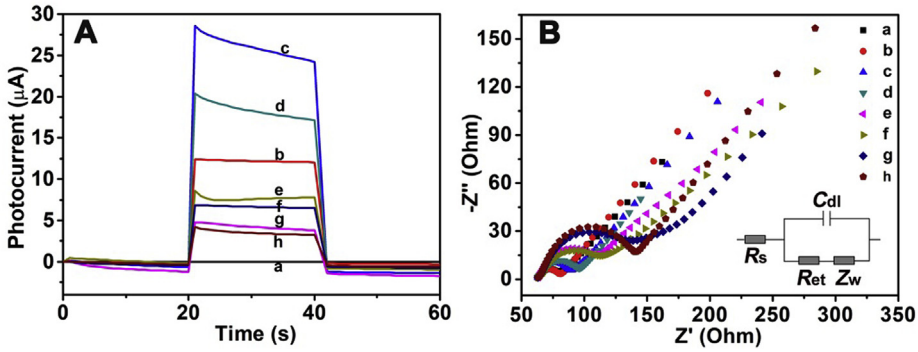

Fig. 3. (A) Photocurrent response and its corresponding (B) EIS Nyquist plots of different modification steps (from a to h): (a) ITO; (b) ITO/TiO_2; (c) ITO/TiO_2/BiOI; (d) ITO/TiO_2/BiOI/CS-GA; (e) ITO/TiO_2/BiOI/CS-GA/Ab_1; (f) ITO/TiO_2/BiOI/CS-GA/Ab_1/BSA; (g) ITO/TiO_2/BiOI/CS-GA/Ab_1/BSA/Aβ; (h) ITO/TiO_2/BiOI/CS-GA/Ab_1/BSA/Aβ/PbS–Au-Ab_2. The EIS experiments were performed without light. The inset in figure B is the equivalent circuit for EIS. The PEC tests were tested in 0.1 mol/L PBS (pH = 7.4) containing 0.1 mol/L AA with 0 V bias voltage and a light source of 430 nm. EIS spectra were performed in 2.5 mmol/L $[Fe(CN)_6]^{3-/4-}$ solution containing 0.1 mol/L KCl.

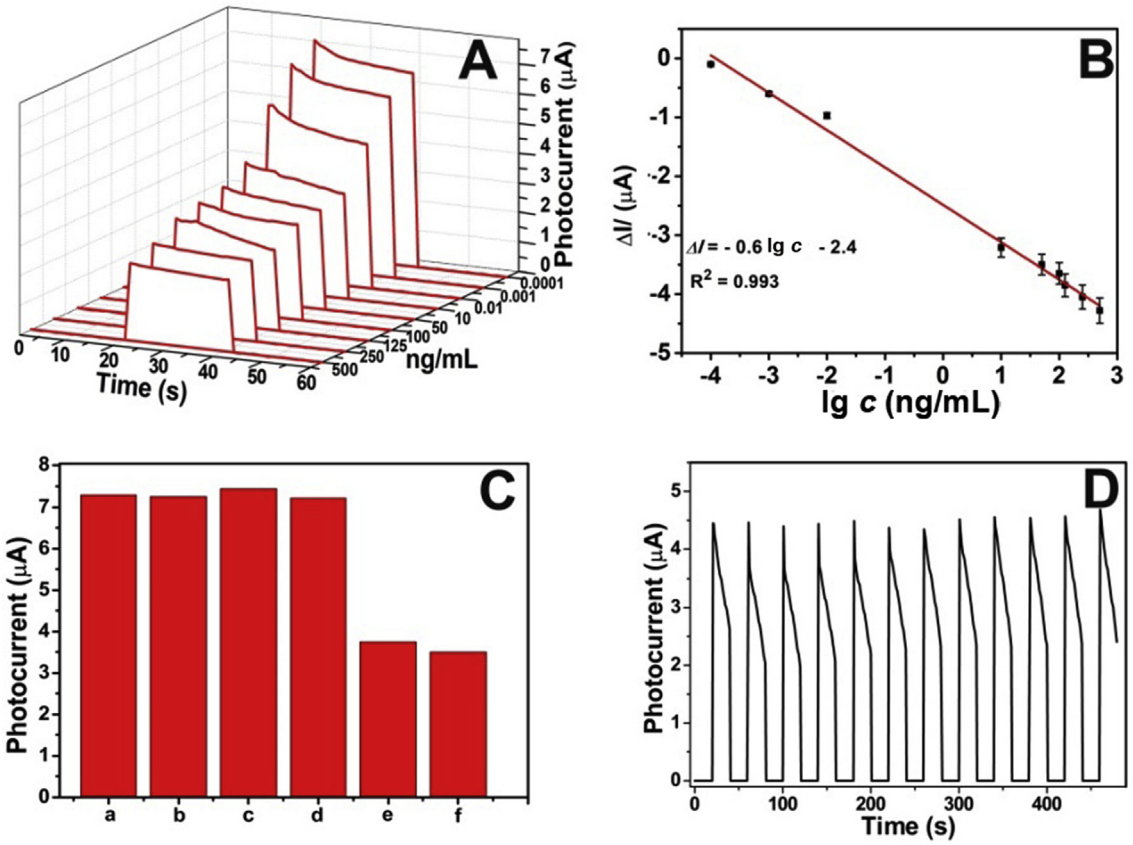

Fig. 4. (A) Photocurrent response of the proposed PEC biosensor with different Aβ concentrations: 0.0001 ng/mL, 0.001 ng/mL, 0.01 ng/mL, 10 ng/mL, 50 ng/mL, 100 ng/mL, 125 ng/mL, 250 ng/mL, 500 ng/mL. (B) The calibration plot of different Aβ concentration determination. ($\Delta I = I - I_0$, I_0 and I are the photocurrent of the biosensor before and after incubation with Aβ, respectively.) (C) Selectivity of the proposed PEC biosensor: (a) blank, (b) PSA (10 ng/mL), (c) CEA (10 ng/mL), (d) IgG (10 ng/mL), (e) Aβ (10 ng/mL), (f) The mixture (containing 10 ng/mL of Aβ, 10 ng/mL of PSA, 10 ng/mL of CEA and 10 ng/mL of IgG). (D) The photocurrent responses of the PEC biosensor for the detection of 10 ng/mL Aβ under repeated "off-on-off" irradiation cycles for 480 s.

cerebrospinal fluid (ACSF) (Shanghai Kingmorn life science Co., Ltd., Shanghai, China). As shown in Table S3, the recovery rate ranged from 96.4% to 104.6%, which demonstrated that the developed biosensor had a promising potential for Aβ determination in clinical diagnostics. Furthermore, to satisfy the need of practical application in future, ELISA method was used as a reference method to assess the proposed PEC method. By using ELISA method and the proposed methods, the Aβ in diluted samples were determined 5 times, respectively. The results were shown in Table S4, which indicated the sufficient precision and high accuracy of the proposed biosensor.

4. Conclusions

A novel signal off PEC sensing platform for the sensitive detection of Aβ was developed by using TiO_2/BiOI heterostructure (p-n) as matrix and PbS–Au heterodimers as the signal quencher. The constructed TiO_2/BiOI heterostructure had superior

photoelectrochemical properties, exhibited double-folds higher photocurrent response than pristine TiO_2. Additionally, by using PbS–Au heterodimers as the signal quencher, the photocurrent response of TiO_2/BiOI could be partly quenched, the reason is that the directly contacted metal (Au)/semiconductor (PbS) junction significantly enhanced the electron separation and transfer rate, and then boosted the electron donor consuming and reduced the output PEC signal. Owing to the introduction of PbS–Au heterodimers, the PEC bioanalysis platform exhibited good performance, with a linear range of 1×10^{-4} to 500 ng/mL, and a low limit of detection (LOD) down to 0.028 pg/mL. Most importantly, the advantages of heterodimers (which containing both semiconductor and noble metal) would offer new design ideas for signal reduction or amplification.

Declaration of competing interest

The authors declare that they have no known competing financial interests or personal relationships that could have appeared to influence the work reported in this paper.

Acknowledgements

We gratefully thank the National Natural Science Foundation of China (Grant no. 21775054), the Natural Science Foundation of Shandong Province (Grant no. ZR2016JL013). Q. Z. Han gratefully thanks the support from Dr. J. H. Feng, Dr. T. T. Wu and Prof. D. Wu.

Appendix A. Supplementary data

Supplementary data to this article can be found online at https://doi.org/10.1016/j.aca.2019.09.041.

References

[1] A. Burns, S. Iliffe, Alzheimer's disease, BMJ 338 (2009).
[2] J.X. Wang, Y. Zhuo, Y. Zhou, H.J. Wang, R. Yuan, Y.Q. Chai, Ceria doped zinc oxide nanoflowers enhanced luminol-based electrochemiluminescence immunosensor for amyloid-β detection, ACS Appl. Mater. Interfaces 8 (2016) 12968–12975.
[3] J. Sepulcre, M.R. Sabuncu, Q. Li, G. El Fakhri, R. Sperling, K.A. Johnson, Tau and amyloid β proteins distinctively associate to functional network changes in the aging brain, Alzheimer's Dementia 13 (2017) 1261–1269.
[4] G.M. McKhann, D.S. Knopman, H. Chertkow, B.T. Hyman, C.R. Jack, C.H. Kawas, W.E. Klunk, W.J. Koroshetz, J.J. Manly, R. Mayeux, R.C. Mohs, J.C. Morris, M.N. Rossor, P. Scheltens, M.C. Carrillo, B. Thies, S. Weintraub, C.H. Phelps, The diagnosis of dementia due to Alzheimer's disease: recommendations from the National Institute on Aging-Alzheimer's Association workgroups on diagnostic guidelines for Alzheimer's disease, Alzheimer's Dementia 7 (2011) 263–269.
[5] S.M. Frost, Y. Kanagasingam, H.R. Sohrabi, K. Taddei, R. Bateman, J. Morris, T. Benzinger, A. Goate, C.L. Masters, R.N. Martins, Pupil response biomarkers distinguish amyloid precursor protein mutation carriers from non-carriers, Curr. Alzheimer Res. 10 (2013) 790–796.
[6] Y. Zhou, H. Wang, Y. Zhuo, Y. Chai, R. Yuan, Highly efficient electrochemiluminescent silver nanoclusters/Titanium oxide nanomaterials as a signal probe for ferrocene-driven light switch bioanalysis, Anal. Chem. 89 (2017) 3732–3738.
[7] J. Han, M. Zhang, G. Chen, Y. Zhang, Q. Wei, Y. Zhuo, G. Xie, R. Yuan, S. Chen, Ferrocene covalently confined in porous MOF as signal tag for highly sensitive electrochemical immunoassay of amyloid-β, J. Mater. Chem-B 5 (2017) 8330–8336.
[8] Z. Luo, Q. Qi, L. Zhang, R. Zeng, L. Su, D. Tang, Branched polyethylenimine-modified upconversion nanohybrid-mediated photoelectrochemical immunoassay with synergistic effect of dual-purpose copper ions, Anal. Chem. 91 (2019) 4149–4156.
[9] Z. Luo, L. Zhang, R. Zeng, L. Su, D. Tang, Near-infrared light-excited core–core–shell UCNP@Au@CdS upconversion nanospheres for ultrasensitive photoelectrochemical enzyme immunoassay, Anal. Chem. 90 (2018) 9568–9575.
[10] W.W. Zhao, J.J. Xu, H.Y. Chen, Photoelectrochemical bioanalysis: the state of the art, Chem. Soc. Rev. 44 (2015) 729–741.
[11] W.W. Zhao, J.J. Xu, H.Y. Chen, Photoelectrochemical immunoassays, Anal. Chem. 90 (2018) 615–627.
[12] K. Zhao, X. Yan, Y. Gu, Z. Kang, Z. Bai, S. Cao, Y. Liu, X. Zhang, Y. Zhang, Self-powered photoelectrochemical biosensor based on CdS/RGO/ZnO nanowire array heterostructure, Small 12 (2016) 245–251.
[13] G. Cai, Z. Yu, R. Ren, D. Tang, Exciton–plasmon interaction between AuNPs/graphene nanohybrids and CdS quantum dots/TiO_2 for photoelectrochemical aptasensing of prostate-specific antigen, ACS Sens. 3 (2018) 632–639.
[14] R. Zeng, Z. Luo, L. Su, L. Zhang, D. Tang, R. Niessner, D. Knopp, Palindromic molecular beacon based Z-scheme BiOCl-Au-CdS photoelectrochemical biodetection, Anal. Chem. 91 (2019) 2447–2454.
[15] Z. Qiu, J. Shu, J. Liu, D. Tang, Dual-channel photoelectrochemical ratiometric aptasensor with up-converting nanocrystals using spatial-resolved technique on homemade 3D printed device, Anal. Chem. 91 (2019) 1260–1268.
[16] X. Wang, R. Xu, X. Sun, Y. Wang, X. Ren, B. Du, D. Wu, Q. Wei, Using reduced graphene oxide-Ca:CdSe nanocomposite to enhance photoelectrochemical activity of gold nanoparticles functionalized tungsten oxide for highly sensitive prostate specific antigen detection, Biosens. Bioelectron. 96 (2017) 239–245.
[17] X. Li, Y. Wang, L. Shi, H. Ma, Y. Zhang, B. Du, D. Wu, Q. Wei, A novel ECL biosensor for the detection of concanavalin A based on glucose functionalized NiCo2S4 nanoparticles-grown on carboxylic graphene as quenching probe, Biosens. Bioelectron. 96 (2017) 113–120.
[18] R. Yang, K. Zou, Y. Li, L. Meng, X. Zhang, J. Chen, Co_3O_4–Au polyhedra: a multifunctional signal amplifier for sensitive photoelectrochemical assay, Anal. Chem. 90 (2018) 9480–9486.
[19] X. Wang, P. Gao, T. Yan, R. Li, R. Xu, Y. Zhang, B. Du, Q. Wei, Ultrasensitive photoelectrochemical immunosensor for insulin detection based on dual inhibition effect of CuS-SiO_2 composite on CdS sensitized C-TiO_2, Sens. Actuators B Chem. 258 (2018) 1–9.
[20] M.J. Li, Y.N. Zheng, W.B. Liang, R. Yuan, Y.Q. Chai, Using p-type PbS quantum dots to quench photocurrent of fullerene–Au NP@MoS_2 composite structure for ultrasensitive photoelectrochemical detection of ATP, ACS Appl. Mater. Interfaces 9 (2017) 42111–42120.
[21] S. Wang, W. Tu, Z. Dai, An ultrasensitive photoelectrochemical bioanalysis strategy for tumor markers based on the significantly enhanced signal of a bismuth oxyiodine microsphere/graphitic carbon nitride composite, Analyst 143 (2018) 1775–1779.
[22] G.L. Wang, J.X. Shu, Y.M. Dong, X.M. Wu, W.W. Zhao, J.J. Xu, H.Y. Chen, Using G-quadruplex/Hemin to "Switch-On" the cathodic photocurrent of p-type PbS quantum dots: toward a versatile platform for photoelectrochemical aptasensing, Anal. Chem. 87 (2015) 2892–2900.
[23] G. Paul, H. Bo, P. Sangyeon, S. Jung Inn, M. Stephen, C. SeungNam, K. Jong Min, Field effect transistors and phototransistors based upon p-type solution-processed PbS nanowires, Nanotechnology 29 (2018), 075202.
[24] D. Kufer, I. Nikitskiy, T. Lasanta, G. Navickaite, F.H.L. Koppens, G. Konstantatos, Hybrid 2D–0D MoS_2–PbS quantum dot photodetectors, Adv. Mater. 27 (2015) 176–180.
[25] L. Gong, H. Dai, S. Zhang, Y. Lin, Silver iodide-chitosan nanotag induced biocatalytic precipitation for self-enhanced ultrasensitive photocathodic immunosensor, Anal. Chem. 88 (2016) 5775–5782.
[26] W.X. Dai, L. Zhang, W.W. Zhao, X.D. Yu, J.J. Xu, H.Y. Chen, Hybrid PbS quantum dot/nanoporous NiO film nanostructure: preparation, characterization, and application for a self-powered cathodic photoelectrochemical biosensor, Anal. Chem. 89 (2017) 8070–8078.
[27] N. Zhao, L. Li, T. Huang, L. Qi, Controlled synthesis of PbS–Au nanostar–nanoparticle heterodimers and cap-like Au nanoparticles, Nanoscale 2 (2010) 2418–2423.
[28] M.A. Mahmoud, W. Qian, M.A. El-Sayed, Following charge separation on the nanoscale in Cu_2O–Au nanoframe hollow nanoparticles, Nano Lett. 11 (2011) 3285–3289.
[29] H. Chen, J.H. Jiang, Y. Huang, T. Deng, J.S. Li, G.L. Shen, R.Q. Yu, An electrochemical impedance immunosensor with signal amplification based on Au-colloid labeled antibody complex, Sens. Actuators B Chem. 117 (2006) 211–218.
[30] H. Jia, W.J. Xiao, L. Zhang, Z. Zheng, H. Zhang, F. Deng, In situ l-hydroxyproline functionalization and enhanced photocatalytic activity of TiO_2 nanorods, J. Phys. Chem. C 112 (2008) 11379–11384.
[31] S. Ng, P. Kuberský, M. Krbal, J. Prikryl, V. Gärtnerová, D. Moravcová, H. Sopha, R. Zazpe, F.K. Yam, A. Jäger, L. Hromádko, L. Beneš, A. Hamáček, J.M. Macak, ZnO coated anodic 1D TiO_2 nanotube layers: efficient photo-electrochemical and gas sensing heterojunction, Adv. Eng. Mater. 20 (2018) 1700589.
[32] T. Butburee, Y. Bai, H. Wang, H. Chen, Z. Wang, G. Liu, J. Zou, P. Khemthong, G.Q.M. Lu, L. Wang, 2D porous TiO_2 single-crystalline nanostructure demonstrating high photo-electrochemical water splitting performance, Adv. Mater. 30 (2018) 1705666.
[33] J. Shu, Z. Qiu, S. Lv, K. Zhang, D. Tang, Plasmonic enhancement coupling with defect-engineered TiO_2–x: a mode for sensitive photoelectrochemical biosensing, Anal. Chem. 90 (2018) 2425–2429.
[34] Z. Qiu, J. Shu, D. Tang, Near-Infrared-to-Ultraviolet light-mediated photoelectrochemical aptasensing platform for cancer biomarker based on core–shell $NaYF_4$:Yb,Tm@TiO_2 upconversion microrods, Anal. Chem. 90 (2018) 1021–1028.
[35] L. Yosefi, M. Haghighi, Fabrication of nanostructured flowerlike p-BiOI/p-NiO heterostructure and its efficient photocatalytic performance in water treatment under visible-light irradiation, Appl. Catal. B Environ. 220 (2018) 367–378.
[36] Y. Feng, C. Liu, H. Che, J. Chen, K. Huang, C. Huang, W. Shi, The highly

improved visible light photocatalytic activity of BiOI through fabricating a novel p–n heterojunction BiOI/WO_3 nanocomposite, CrystEngComm 18 (2016) 1790–1799.
[37] J.C. Wang, H.C. Yao, Z.Y. Fan, L. Zhang, J.S. Wang, S.Q. Zang, Z.J. Li, Indirect Z-scheme BiOI/g-C_3N_4 photocatalysts with enhanced photoreduction CO_2 activity under visible light irradiation, ACS Appl. Mater. Interfaces 8 (2016) 3765–3775.
[38] L. Sun, L. Xiang, X. Zhao, C.J. Jia, J. Yang, Z. Jin, X. Cheng, W. Fan, Enhanced visible-light photocatalytic activity of BiOI/BiOCl heterojunctions: key role of crystal facet combination, ACS Catal. 5 (2015) 3540–3551.
[39] Y. Zhang, Q. Pei, J. Liang, T. Feng, X. Zhou, H. Mao, W. Zhang, Y. Hisaeda, X.M. Song, Mesoporous TiO_2-based photoanode sensitized by BiOI and investigation of its photovoltaic behavior, Langmuir 31 (2015) 10279–10284.
[40] G. Dai, J. Yu, G. Liu, Synthesis and enhanced visible-light photoelectrocatalytic activity of p–n junction BiOI/TiO_2 nanotube Arrays, J. Phys. Chem. C 115 (2011) 7339–7346.
[41] D. Wu, Y. Wei, X. Ren, X. Ji, Y. Liu, X. Guo, Z. Liu, A.M. Asiri, Q. Wei, X. Sun, $Co(OH)_2$ nanoparticle-encapsulating conductive nanowires array: room-temperature electrochemical preparation for high-performance water oxidation electrocatalysis, Adv. Mater. 30 (2018) 1705366.